# Absence of spin-flip transition at the Cr(001) surface: A combined spin-polarized scanning tunneling microscopy and neutron scattering study

T. Hänke, S. Krause, L. Berbil-Bautista, M. Bode,* and R. Wiesendanger

*Institute of Applied Physics and Microstructure Research Center, University of Hamburg, Jungiusstrasse 11, D-20355 Hamburg, Germany*

V. Wagner

*Physikalisch-Technische Bundesanstalt (PTB), Bundesallee 100, D-38116 Braunschweig, Germany*

D. Lott and A. Schreyer

*Institut für Werkstoffforschung, GKSS Forschungszentrum, Max-Planck-Strasse 1, D-21502 Geesthacht, Germany*

The spin-density wave (SDW) on Cr(001) has been investigated at temperatures between 20–300 K by means of spin-polarized scanning tunneling microscopy (SP-STM). Although neutron-scattering data measured on the same crystal clearly show a spin-flip transition from a transversal (T)-SDW to a longitudinal (L)-SDW at the expected spin-flip (SF) temperature $T_{SF} = 123$ K, no change was found on the Cr(001) surface with SP-STM. Throughout the entire temperature range the Cr(001) surface maintains a topological antiferromagnetic order with an in-plane magnetization that inverts between adjacent atomically flat terraces separated by monatomic step edges. The experimental results are interpreted by an absence of a spin-flip transition in the near-surface region probably driven by the surface anisotropy. The continuous connection of the surface T-SDW to the bulk L-SDW is accomplished by the formation of a 90° domain wall just below the surface.

## I. INTRODUCTION

Since the discovery of an incommensurate spin-density wave (I-SDW) in 1959,[1] the complex magnetic structure of Cr has been of continuing interest. As the SDW in bulk chromium has been intensively studied it is generally accepted as a typical example of how the electronic structure and the topology of the Fermi surface may influence magnetism in itinerant systems. Arising from its role in exchange-coupled Fe/Cr bilayers and superlattices,[2,3] which feature interesting magnetic effects such as giant magnetoresistance,[4,5] the attention was recently drawn to the magnetic properties of Cr at reduced dimensionality. Proximity effects of Cr with ferromagnetic layers, thin Cr films, and the Cr surface itself were intensively studied.[6] As the physical properties of Cr exhibit quite complex phenomena we refer to the comprehensive review article by Fawcett.[7] Here, only the properties that are of direct concern to the present work are briefly mentioned.

Chromium has a bcc structure with a lattice parameter of $a_{Cr} = 2.884$ Å in the paramagnetic state. Cr is a $3d$ transition metal and has to be considered as an itinerant antiferromagnet with a Néel transition temperature $T_N = 311$ K in the bulk. Pure Cr exhibits an incommensurate spin-density wave, which originates from the nesting of the Fermi surface. It consists of a static sinusoidal modulation of the magnetic moments with a period $L$ between $27a_{Cr}$ ($\approx 7.8$ nm) at room temperature and $21a_{Cr}$ ($\approx 6.1$ nm) at 10 K.[6,7] Two different modifications exist, i.e., the transverse (T) and the longitudinal (L) SDW below the Néel temperature $T_N = 311$ K and the spin-flip (SF) temperature $T_{SF} = 123$ K, respectively. While in the case of the T-SDW, the magnetic moment $\vec{\mu}$ is perpen-

dicular to the propagation direction $\vec{Q}$ of the SDW ($\vec{\mu} \perp \vec{Q}$), the longitudinal SDW exhibits a parallel configuration ($\vec{\mu} \parallel \vec{Q}$). For both SDW types the propagation vector $\vec{Q}$ points along one of the three possible $\langle 100 \rangle$ directions. Since all three $\langle 100 \rangle$ directions are equivalent within the crystal bulk, they coexist at equal probability. Because of spin-orbit-induced magnetoelastic interactions the magnetic phase transitions are accompanied with a change of the crystal symmetry. Namely, the paramagnetic bcc structure transfers into an orthorhombic crystal symmetry below $T_N$ and a tetragonal symmetry is found for the L-SDW.

This situation may change completely if the symmetry is reduced by introducing a surface or an interface. In spite of its antiferromagnetic bulk structure, ferromagnetic order and an increased magnetic moment have been predicted for a perfect Cr(001) surface without any steps.[8] Early experimental data were rather contradictory. Angle- and energy-resolved photoemission indicated that the Cr surface states are exchange split,[9] which is consistent with the theoretical prediction of ferromagnetically ordered terraces, but no net magnetization was found by spin-resolved photoemission.[10] This apparent inconsistency was explained by Blügel *et al.*,[11] who calculated that the magnetic moments of any atomically flat terrace couple parallel, but—as a result of the antiferromagnetism of Cr—adjacent terraces are magnetized antiparallel. Since this model implies a close link between the surface topology and the magnetic structure the magnetic state of Cr(001) was called "topological antiferromagnetism."

Since the magnetization direction alternates laterally and vertically with periodicities, which are given by the average terrace width and the interlayer distance, respectively, lateral and vertical averaging leads to the cancellation of the spin

signal, making a direct experimental proof of topological antiferromagnetism extremely difficult. A suitable experimental method must have a high lateral resolution (better than the average terrace width) as well as a high surface sensitivity in order to exclusively probe the magnetization of one particular surface layer. Both conditions are fulfilled by spin-polarized scanning tunneling microscopy (SP-STM) and spectroscopy (SP-STS).[12–16] Recent studies delivered the following picture of the Cr(001) surface magnetic structure at room temperature for $T > T_{SF}$.[13–15] In fact, the magnetic structure of the perfect Cr(001) surface is adequately described by the model of the topological antiferromagnetism. A direct comparison of magnetically in-plane sensitive differential conductance d$I$/d$U$ maps with simultaneously measured topographic STM images revealed that the d$I$/d$U$ signal abruptly changes between two discrete levels whenever a monatomic step edge is crossed. This variation is caused by the fact that adjacent terraces have opposite in-plane magnetization directions. Moreover, it was found that the magnetization direction of adjacent Cr(001) terraces persistently alternates even over a large number of terraces without any change in the d$I$/d$U$ contrast.[14] This is somewhat surprising as the incommensurate sinusoidal modulation of the SDW may cause phase slips as found previously for Cr wedges on Fe(001) whiskers.[17]

Both findings, the in-plane orientation of the magnetization as well as the absence of any phase slip or long-wavelength modulation of the surface magnetic moment, strongly reduce the number of possible configurations of the SDW at the Cr(001) surface. First, since the above-mentioned measurements were performed at room temperature where the SDW is transversal ($\vec{\mu} \perp \vec{Q}$) and since an in-plane magnetization was found,[14] it can be concluded that the propagation vector $\vec{Q}$ of the SDW is always oriented perpendicular to the surface plane. This so-called single $\vec{Q}$ state in the near-surface region was also found by x-ray scattering,[18–20] neutron-scattering,[19,20] and perturbed angular correlation spectroscopy studies[21] performed at various Cr(001) layered systems.[22] On Cr(110) a similar situation was also found by means of low-temperature STM[23] for the charge-density wave (CDW), which is closely connected to the SDW.[24] Second, in order to explain the constant size of the surface magnetic moment, the surface SDW cannot be a simple extension of the bulk SDW. Two possible spin configurations are schematically sketched in Fig. 1. The first possibility is characterized by a T-SDW that is slightly shifted between adjacent terraces to maximize the magnetic moment for every individual (001) surface layer. This situation is schematically represented in Fig. 1(a). A second modification, shown in Fig. 1(b), leaves the bulk SDW unchanged, but the coupling of the Cr(001) surface layer to the first subsurface layer varies such that the surface magnetic moment is maximized for any terrace. In principle, both interpretations are consistent with the theoretical calculation mentioned above that predict an enhanced magnetic moment for the Cr(001) surface,[25] similar to recent observations on Cr(110).[26] In either case the magnetic frustration certainly leads to an enhanced exchange energy. While in the former model [Fig. 1(a)] small-angle domain walls are formed at
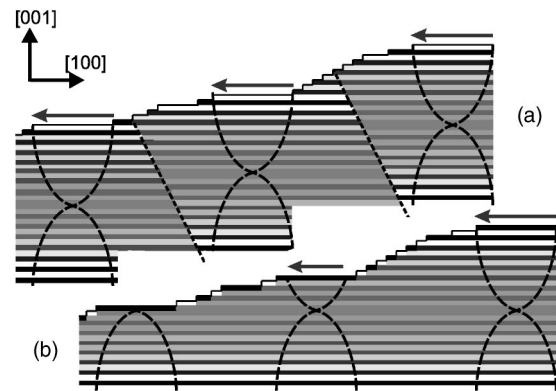


FIG. 1. Two different models of the Cr T-SDW at the surface. (a) The SDW exhibits a maximal magnetic moment for every individual (001) surface layer. In this case small-angle domain walls must exist being oriented perpendicular to the surface. (b) The bulk SDW is perfectly maintained up to the first subsurface layer. Only the coupling between the surface layer and the first subsurface layer is frustrated in order to maximize the surface magnetic moment at the surface.

any step edge between two terraces, the latter model implies a frustration of the exchange interaction between the surface and the first subsurface layer.

Thus far, the observed properties of the surface magnetic structure of Cr(001) were obtained at room temperature above the spin-flip temperature $T_{SF}$. The above-described room-temperature spin configuration with its in-plane magnetization and the resulting perpendicular alignment of the propagation vector $\vec{Q}$ relative to a Cr(001) surface without steps is shown in another representation in Fig. 2(a). The maximum of the T-SDW is located at the surface giving rise to a maximal surface magnetic moment. The question arises how the bulk spin-flip reorientation influences the magnetic structure of the Cr(001) surface below $T_{SF}$ when the SDW becomes longitudinally polarized. There are two simple scenarios that are sketched in Fig. 2(b) and 2(c): Either the direction of the magnetic moment $\vec{\mu}$ or the propagation vector $\vec{Q}$ must be modified. In the former case $\vec{Q}$ remains perpendicular to the (001) surface. Furthermore, as for $T > T_{SF}$, the surface magnetic moment remains maximal and the SDW antinode is pinned at the surface. Similar to the situation sketched in Fig. 2(a) the surface magnetic order exhibits topological antiferromagnetism but with an out-of-plane magnetization of the surface. In the second scenario $\vec{Q}$ may be oriented parallel to the (001) surface as shown in Fig. 2(c). In this case the surface magnetization remains in-plane, but we shall no longer observe topological antiferromagnetism. Instead, a modulation of the magnetic moment with the period $L$ of the SDW should be visible on atomically flat terraces. As we will show in the course of this paper both models are inconsistent with the experimental data, which will be presented later on.

In this paper, we report on a combined temperature-dependent investigation of the Cr bulk SDW by neutron scattering and of the Cr(001) surface by SP-STS performed on the same Cr single crystal. The neutron-scattering experiments confirm that—in spite of some mechanical strain
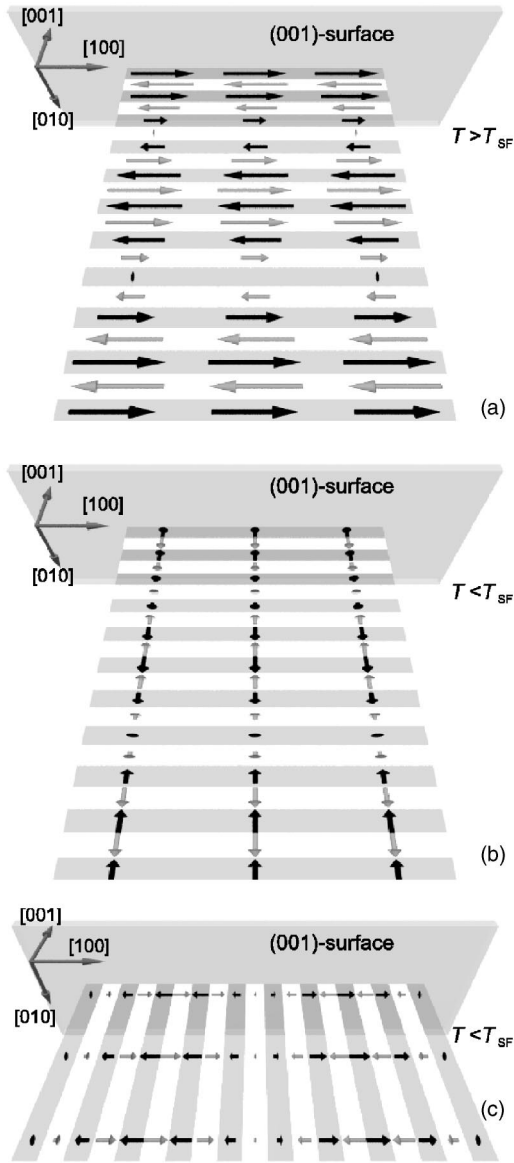
FIG. 2. Schematic scenarios of the spin configuration of the Cr SDW at different temperatures. (a) At $T > T_{SF}$ the T-SDW propagates perpendicular toward the Cr(001) surface. The maximum of the SDW is located at the surface, and the surface layer has an in-plane ferromagnetic order. Below $T_{SF}$ the $\vec{Q}$ vector of the L-SDW has two possible orientations relative to the surface: (b) perpendicular, with a maximum at the surface resulting in an out-of-plane ferromagnetic surface layer or (c) parallel to the surface with a modulation of the surface magnetic moment within the (001) surface. As will be shown in the course of this paper both models are inconsistent with the experimental data.

caused by the clamping of the crystal onto the sample holder—the incommensurable SDW dominates the bulk magnetic structure and that the spin-flip transition occurs at the expected temperature. In contrast, no transition is observed on the surface, but topological antiferromagnetic order with the magnetization lying in the surface plane is found by SP-STS within the entire studied temperature range of $23 \text{ K} \leqslant T \leqslant 293 \text{ K}$. The paper is organized as follows. In Sec. II we outline the experimental setup of the neutron-scattering

experiments. Furthermore, the SP-STS experimental setup, including tip and sample preparation procedures and the contrast mechanism, are described. After describing the characterization of the magnetic bulk properties of our Cr(001) single crystal in Sec. III A by neutron scattering, we will present temperature-dependent SP-STS measurements of Cr(001) in Sec. III B. First SP-STS measurements showing the topological antiferromagnetism as found on clean Cr(001) surfaces above $T_{SF}$ are presented. Then the temperature-dependent magnetic structure of the Cr(001) surface is studied by SP-STS between room temperature and $T = 23$ K. Finally, in Sec. IV we discuss the results and compare them to measurements obtained for epitaxially grown Cr(001) films.

## II. EXPERIMENTAL SETUP

### A. Neutron scattering

In the past the spin structures and phase transitions of Cr were primarily studied by elastic neutron scattering. It is a well-established technique that is used here to complement the SP-STS characterization of our Cr single crystal by probing its SDW bulk behavior. The scattering cross section of an unpolarized neutron beam with a spin-density wave $\vec{M}(\vec{r})$ is given by[7,27,28]

$$\frac{d\sigma}{d\Omega} = |\vec{M}_q|^2 \sin^2 \Theta_q \cdot \delta(\vec{q} + \vec{q}_{\pm} - \vec{G}_{bcc}), \quad (1)$$

where $\Theta_q$ is the angle between the magnetization $\vec{M}(\vec{r})$ and the scattering vector $\vec{q}$, $\vec{M}_q$ is the Fourier component of $\vec{M}(\vec{r})$ corresponding to the scattering vector $\vec{q} = \vec{k}' - \vec{k}''$, $\vec{q}_{\pm} = \vec{G}_{\{001\}} \times (1 - \epsilon)$ is the wave vector of the spin-density wave with $\epsilon$ as a measure of the deviation from the commensurability, and $\vec{G}_{bcc}$ are the reciprocal lattice vectors for the allowed bcc reflections. The $\delta$ function in Eq. (1) indicates that the intensity from the magnetic scattering is only observed at positions in reciprocal space for which $\vec{q} = \vec{G}_{bcc} - \vec{q}_{\pm}$. The existence of incommensurate SDWs (i.e., $\epsilon \neq 0$) results in characteristic satellite peaks in the vicinity of the structurally forbidden bcc reflections. The bottom panel of Fig. 3 illustrates possible satellite reflections for neutron scattering in reciprocal space originating from SDW structures in Cr.

Two criteria need to be considered in order to determine the propagation direction and polarization of the SDW in Cr, i.e., $\vec{q}_{\pm}$ and $\vec{M}_q$. The orientation and magnitude of $\vec{q}_{\pm}$ corresponds to the vector between any of the satellite peak positions and the next-nearest allowed bcc reciprocal-lattice point which identifies the propagation direction of the SDW. Second, the magnetic neutron-scattering cross section only yields intensity for components of the magnetization vector $\vec{M}_q$ perpendicular to the scattering vector. With several selected scans in orthogonal directions these criteria can be used to unambiguously determine the nature of the SDW. Figure 3 provides a summary of the conditions for the observation of satellite reflections in various directions because of the selection criteria. The period length $\Lambda_{SDW}$ of the SDW

| SDW-mode | (001) L-satellite | (001) K-satellite | (010) L-satellite | (010) K-satellite |
|---|:---:|:---:|:---:|:---:|
| out-of-plane longitudinal spins out-of-plane | ○ | ○ | ● | ○ |
| out-of-plane transversal spins in-plane | ● | ○ | ● | ○ |
| in-plane longitudinal spins in-planel | ○ | ● | ○ | ○ |
| in-plane transversal spins in-plane | ○ | ● | ○ | ● |
| in-plane transversal spins out-of-plane | ○ | ○ | ○ | ● |
| positions of the satellite reflections around the [010] and [001] Bragg reflections in the reciprocal space | (diagram) | (diagram) | (diagram) | (diagram) |

FIG. 3. (Bottom row) Overview of neutron-scattering geometries with satellite reflections as they occur for different longitudinal and transverse incommensurate spin-density waves. (Top rows) Lookup table with filled and empty circles indicating the presence and absence of satellite reflections for certain spin-density waves (adapted from Ref. 20).

can be determined from the distance of the satellite position to the next-nearest $\vec{G}_{\{001\}}$ position with

$$\Lambda_{\mathrm{SDW}} = \frac{a_{\mathrm{Cr}}}{\epsilon}, \qquad (2)$$

where $a_{\mathrm{Cr}}$ is the lattice constant of Cr.

In case of $\epsilon = 0$ ($\Lambda_{\mathrm{SDW}} = \infty$) the Cr SDW is commensurate, resulting in a simple antiferromagnetic ($AF_0$) structure with the corner atoms on the Cr bcc lattice antiparallely aligned to the center atoms. According to the discussion above, this leads to peaks at the $\{001\}$ positions in the neutron- scattering spectra, whereas the incommensurate SDW creates maxima in the proximity of the $\{001\}$ positions. Thus, the distinction of the commensurate and incommensurate Cr-SDW by neutron scattering is straightforward.

The experiments were carried out at POLDI, a neutron diffractometer, situated on a thermal neutron guide at the Geesthacht Neutron Scattering Facility (GENF) at GKSS using monochromatic neutrons with a wavelength of 0.18 nm. Higher harmonics, which would be reflected by POLDI's graphite monochromator potentially causing spurious peaks at the $\{001\}$ positions, were completely suppressed by the use of a velocity selector. A cryostat was employed to set the sample temperature within the required range between 13 and 350 K.

### B. Cr preparation

All experiments were performed using the same (001)-oriented disk-shaped Cr single crystal, which has a 10 mm diam and 0.8 mm thickness. It is rigidly mounted with a Tantalum frame spot-welded on top of the tungsten sample holder. As already described in previous publications,[13,14] the Cr(001) single crystal was cleaned by prolonged cycles of $Ar^+$ ion etching at elevated temperatures ($T \leqslant 1100$ K) and subsequent annealing for 20–30 min at $T = 1150$ K. Compared to early experiments, the amount of residual impurities could be reduced significantly by using an $Ar^+$ ion gun with a mass filter (Wien filter). Eventually, the Cr(001) surface contains less than 2% of carbon (C). All other elements, such as O, S, and N, are below the Auger

electron spectroscopy (AES) sensitivity limit of $\leqslant 1\%$. The cleanliness of the surface is corroborated by the existence of a $d_{z^2}$-like surface state close to the Fermi level $E_F$, which shows up as a distinct peak in scanning tunneling spectroscopy measurements[13,14] and is characteristic for clean bcc(001) surfaces.[25]

### C. Spin-polarized scanning tunneling microscopy

The SP-STM experiments were performed in an ultrahigh vacuum (UHV) system with two separate chambers: (i) a preparation chamber for the tip and sample treatment and (ii) an analysis chamber for sample surface characterization by means of low-energy electron diffraction (LEED) and Auger electron spectroscopy. Furthermore, a satellite of the analysis chamber contains a home-built scanning tunneling microscope (STM), which operates at temperatures between 20 and 350 K. It has a maximum scan range of $8 \times 8$ $\mu m^2$ at room temperature (RT) and $5 \times 5$ $\mu m^2$ at 20 K. The core of the STM is similar in design to the microscope described in Ref. 29 and is equipped with a tip exchange mechanism. In contrast to some commercially available variable-temperature scanning tunneling microscopes (VT-STM), where only the sample is cooled but the tip always remains at RT, the entire microscope including tip and scanner is cooled in our setup. This is performed by connecting the STM via a highly flexible copper braid to the cold finger of a continuous-flow liquid He cryostat. The STM is situated inside a radiation shield that is connected with a second copper braid to the outer radiation shield of the cryostat being cooled by the exhaust He. For vibration isolation the entire setup is mounted on top of an eddy current damping stage. A resistive heater inside the flow cryostat allows the precise variation of temperature. The base pressure in both chambers is in the low $10^{-11}$ torr range.

We used polycrystalline W tips that were electrochemically etched *ex situ* and cleaned *in vacuo* by a high-temperature flash at $T \geqslant 2200$ K. Spin-resolved studies were carried out by using *in situ* prepared Fe-coated W tips. Details of the tip-preparation procedure are described in Refs. 16 and 30. From previous experiments, which partly have been performed in an external magnetic field, we know that
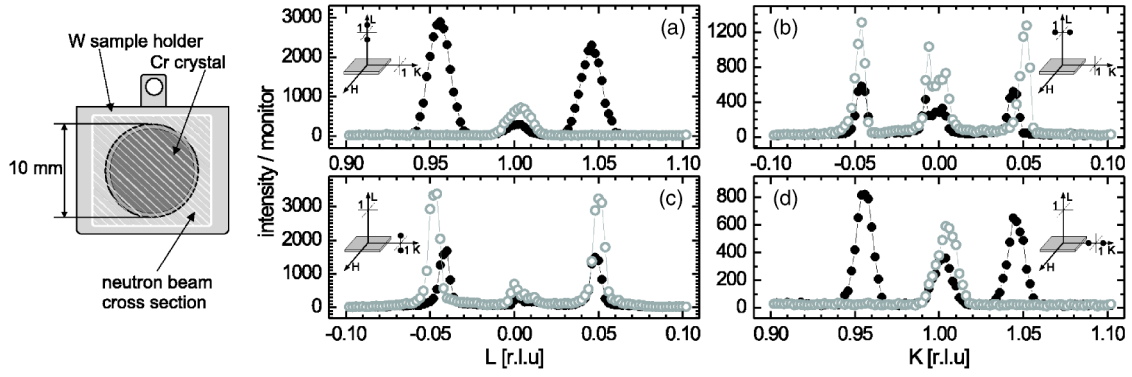
FIG. 4. Neutron-scattering data of Cr(001) measured with neutrons illuminating the entire crystal (see hatched area in drawing on the left). Measurement temperatures are $T_{SF}<T=200$ K (filled circles) and $T_{SF}>T=20$ K (open circles) to explore the propagation directions and polarizations of the spin-density waves. The sequence of (a)–(d) follows the same order as the columns of Fig. 3. The scattering geometries are sketched as insets.

Fe-coated W tips are preferentially magnetized perpendicular to the tip axis,[30,31] i.e., parallel to the sample's surface plane. With both tip and sample held at the same temperature $T$, maps of the spin-resolved differential tunneling conductance $dI/dU$ (magnetic signal) were recorded simultaneously to the constant-current images (topography) by adding a modulation voltage $U_{mod}=10$ mV$_{rms}$ to the sample bias $U$ and detecting the $dI/dU$ signal by lock-in technique in closed-feedback circuit configuration.

To image the magnetic structure of the Cr(001) surface, the above-mentioned $d_{z^2}$-like surface state can be utilized as it exhibits a spin polarization of about 20% because it is the minority-spin part of an exchange split $d$ band.[12,13] As we use Fe-coated W tips both electrodes are spin-polarized and the differential conductance measured at the location $\vec{r}$ on the surface for a sample bias voltage $U_0$ can be written as[32]

$$\frac{dI}{dU}(\vec{r},U_0)_{SP}=C(1+P_sP_t\cos\theta), \qquad (3)$$

where $C=dI/dU(\vec{r},U_0)_{sa}$ is the spin-averaged part of the differential conductance, $P_t=P_t(E_F-eU_0)$ and $P_s=P_s(E_F+eU_0)$ is the spin polarization of the tip and the sample at the energy $E_F\pm eU_0$, respectively. The angle $\theta=\theta[\vec{M}_s,\vec{M}_t(\vec{r})]$ is enclosed by the tip magnetization $\vec{M}_t$ and the local sample magnetization $\vec{M}_s(\vec{r})$ below the tip apex. For an electronically homogeneous surface, $C$ and $P_s$ are independent of the location $\vec{r}$ on the surface. Therefore, any lateral variation of $dI/dU$ signal is caused by the $\cos\theta$ term, which—at a fixed magnetization direction of the tip—only depends on the local orientation of the sample magnetization $\vec{M}_s(\vec{r})$. Accordingly, the $dI/dU$ signal is sensitive to the local electron spin density of the sample surface. Since the atomic structure of the cluster at the tip apex determines its (spin-dependent) electronic structure and $P_t$, just as $P_s$, is a bias voltage-dependent quantity, the bias voltage at which the product $P_tP_s$ becomes maximal cannot be predicted and varies between different tips prepared in different experimental runs.

All "topographic" STM data shown below have been plane fitted on atomically flat terraces to correct for the tilt of the sample. In order to enhance the contrast we mixed the tip height $z$ and its derivative $dz/dx$ with respect to the fast scan direction $x$. This image processing suggests a topography that is illuminated by an invisible light source from the left.

## III. RESULTS

### A. Neutron scattering

The properties of the Cr SDW are highly sensitive to the sample quality. For example, elastic strain can cause the SDW to change from commensurate to incommensurate yielding qualitatively different neutron-scattering spectra. In the case of the Cr crystal examined here mechanical strain may result from the mounting procedure (see Sec. II B). In particular, locations where the Cr sample and the tantalum foil touch are more susceptible to irregularities with crystalline imperfections (ripples) visible to the naked eye.

In order to examine the SDW bulk behavior of the Cr crystal, neutron-scattering experiments were carried out. The white hatched area in the left sketch of Fig. 4 shows the area illuminated with the neutron beam in the first measurements. This includes the Cr crystal and some of the surrounding Ta frame. The resulting scans are shown in Figs. 4(a)–4(d). At 200 K, well above the spin-flip temperature $T_{SF}$, satellite reflections are observed along the $K$ and $L$ direction in the vicinity of the (010) and the (001) forbidden Bragg positions for the structural reflections.

As the dark gray shaded components in Fig. 3 indicate, the occurrence of the satellites is characteristic for a transverse I-SDW as expected above $T_{SF}$. At 20 K, far below the spin-flip temperature, the satellites in the vicinity of the (001) position along the $K$ direction in Fig. 4(b) and the satellites along the $L$ direction next to the (010) position in Fig. 4(c) remain present, but the satellites in the proximity of the (001) and (010) positions along the $L$ and $K$ direction, respectively, in Fig. 4(a) and 4(d) disappear. The result is highlighted in light gray in Fig. 3 and corresponds to the expected behavior for a longitudinal I-SDW in the $K$ and $L$ directions. From the peak positions in Fig. 4(b), the period length of the SDW is calculated to be $\Lambda_{SDW}=70\pm4$ Å at
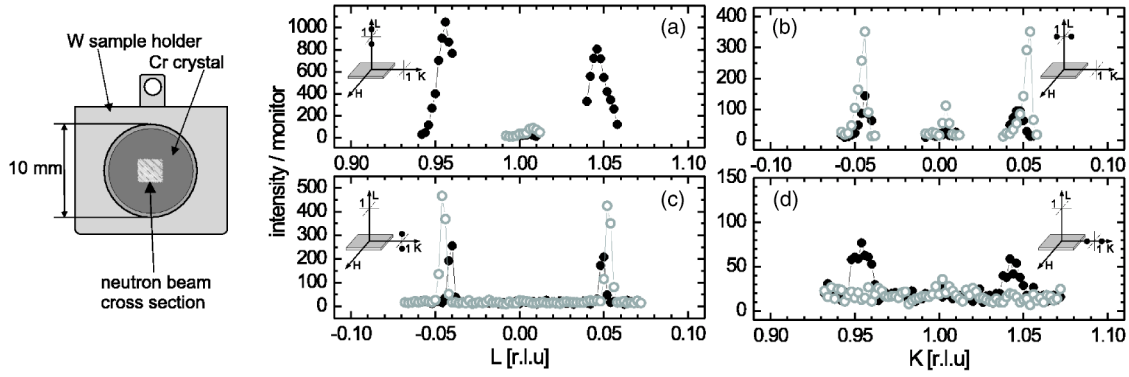
FIG. 5. Neutron-scattering data of Cr(001) measured with the neutron beam confined to the central region of the Cr crystal (see hatched area in drawing on the left). Measurement temperatures are $T_{SF} < T = 200$ K (filled circles) and $T_{SF} > T = 20$ K (open circles) to explore the propagation directions and polarizations of the spin-density waves. The sequence of (a)–(d) follows the same order as the columns of Fig. 3. The scattering geometries are as sketched as insets.

200 K and $\Lambda_{SDW} = 64 \pm 4$ Å at 20 K using Eq. (2), which is in good agreement with Ref. 33.

In addition to the scans at 20 and 200 K, the intensity of the satellite reflection in the $K$ direction close to the (010) position was recorded during the cooldown process (data not shown here). It was found that the intensity drops rapidly at about $T = 125 \pm 5$ K, agreeing well with the expected $T_{SF}$ of 123 K. By heating the sample above the bulk Néel temperature of $T_N = 311$ K, all peaks related to magnetic scattering disappear (data not shown here), indicating that the Cr sample became paramagnetic.

Along with the satellite peaks in Fig. 4, peaks owed to magnetic scattering also appear directly at the (010) and the (001) Bragg positions. These reflections arise from magnetic scattering from a commensurate SDW (AF$_0$ phase). The appearance of the AF$_0$ phase can be attributed to the mechanical strain, which is expected to be present at the crystal edges where the Ta foil presses onto the Cr surface. In order to check whether the AF$_0$ phase pervades the whole sample or is only restricted to the edges of the sample, the beam size of the neutron beam was confined by a Lithium plated aperture to an area of $2 \times 2$ mm$^2$, narrowing the illuminated spot to the center of the Cr crystal (see white hatched area in the left sketch of Fig. 5). Figure 5 shows the corresponding neutron-scattering scans. Qualitatively, the satellite reflections exhibit the same behavior as without an aperture, i.e., the existence of a transverse I-SDW above and a longitudinal I-SDW below $T_{SF}$. In contrast to the previous data taken by averaging over the entire crystal, however, the intensities of the commensurate SDWs are now dramatically reduced relative to the incommensurate satellites. The reflection at the (010) position has completely disappeared [see Figs. 5(c) and 5(d)]. Obviously, the incommensurate SDW phase is dominant in the center of the Cr crystal, the same position at which the SP-STS measurements were carried out later. Similarly, the still visible but very weak commensurate SDW reflections at the (001) position is found to be minimal, when the neutron beam hits the sample center [see Figs. 5(a) and 5(b)]. The remaining intensity at (001) can be attributed to the fact that during a scan the projection of the neutron beam onto the sample surface actually deviates from the square form shown in Fig. 5 toward a rectangular shape, hitting off-center areas

of the sample, leading to minor contributions from areas closer to the edges of the Cr crystal. This effect is significantly weaker for the scattering geometry of Figs. 5(c) and 5(d), than for Figs. 5(a) and 5(b), explaining the stronger peaks at the commensurate (001) position in the latter case.

### B. *T*-dependent SP-STS

Although a commensurate SDW (AF$_0$ phase) is present in our Cr crystal—presumably because of the elastic strain caused by the clamping mechanism—our neutron-scattering experiments revealed that the incommensurate SDW dominates the central region of the sample surface where the SP-STM measurements are performed. In the following we present surface-sensitive spin-polarized STS measurements, starting with a brief synopsis of a typical Cr(001) surface at temperatures between $T_N$ and $T_{SF}$.

Figure 6(a) shows the topography of a clean Cr(001) surface measured at $T = 200$ K. Ten terraces can be recognized that descend from the lower-left to the upper-right edge of the image. The section in the upper panel of Fig. 6(c) has been drawn along the surface region indicated by the black box in Fig. 6(a). It reveals that adjacent terraces are separated by monatomic steps of $1.44 \pm 0.08$ Å height. This terrace-and-step structure, which is found on any real surface, is the result of a slight miscut (locally about 0.04°, averaged over the whole sample approximately 0.15°) with respect to the ideal (001) surface. Figure 6(b) shows the simultaneously acquired map of the differential conductance $dI/dU$ as measured with an magnetically in-plane sensitive Fe-coated tungsten tip. Obviously, the strength of the $dI/dU$ signal abruptly changes between two discrete levels at any step edge as expected for a surface that exhibits topological antiferromagnetism. This signal variation is the result of spin-polarized tunneling between the magnetic sample and the magnetic tip. The section of the $dI/dU$ signal in the lower panel of Fig. 6(c) confirms that there are only two levels of the $dI/dU$ signal, denoted A and B. Apart from these step edges two further defects in form of screw dislocations are visible in the lower-right part of Fig. 6(a) and are marked by arrows. Screw dislocations lead to the formation of semi-infinite step edges that start at the respective point of inter-
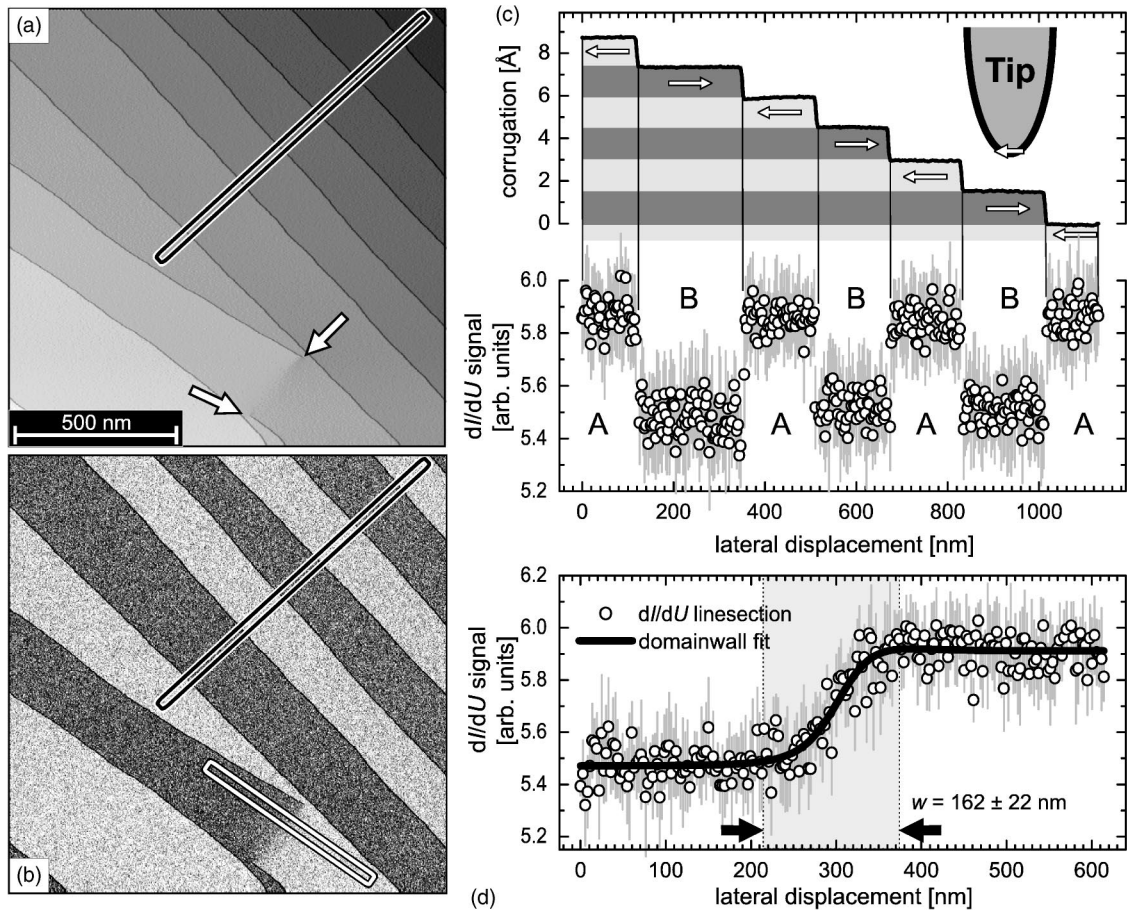
FIG. 6. (a) Constant-current STM image of the clean Cr(001) surface showing several terraces separated by monatomic steps. The data were obtained at a temperature of $T=200$ K with a magnetic Fe-coated probe tip using a tunneling current $I=0.3$ nA and a sample bias voltage $U=-100$ mV. (b) Spin-polarized spectroscopic image of the $dI/dU$ signal of the same surface region shown in (a). The right panels show averaged sections drawn along the boxes, whereas (c) corresponds to the line perpendicular to the step edges (black box) and (d) to the one across the domain wall (white box).

ception of the dislocation line with the Cr(001) surface plane. Obviously, the Cr(001) surface cannot exhibit the perfect topological antiferromagnetic order around a screw dislocation. Instead, a domain wall is formed between the two screw dislocations. A more detailed analysis of domain walls induced by dislocations on the Cr(001) surface can be found in Ref. 15. To determine the domain-wall width we have drawn an average profile of the $dI/dU$ signal along the white line section in Fig. 6(b). The result is plotted in Fig. 6(d). A quantitative analysis is performed on the basis of continuum micromagnetic theory[34] by fitting the measured data with a standard domain-wall profile

$$y(x) = y_0 + y_{SP} \cos(\arccos\{\tanh[(x - x_0)/(w/2)]\} + \phi),$$

(4)

where $y(x)$ is the $dI/dU$ signal measured at position $x$, $x_0$ is the position of the domain wall, $w$ the domain wall width, and $y_0$ and $y_{SP}$ are the non-spin-polarized and spin-polarized part of the $dI/dU$ signal, respectively. $\phi$ is the azimuth between the tip and sample magnetization. For this particular domain wall the best fit is achieved with $\phi=31°$, leading to a width of $w=162\pm10$ nm being in good agreement with

former results, which showed a domain-wall width of 120–170 nm.[13,15]

It is a rather obvious but still open question how the magnetic structure of the Cr(001) surface behaves when crossing the spin-flip temperature. Figure 7 shows a series of six SP-STS measurements of the Cr(001) surface taken at temperatures between room temperature ($T=293$ K) and 23 K, thereby crossing the spin-flip temperature $T_{SF}=123$ K. The simultaneously measured topography and spin-resolved $dI/dU$ map are presented for each temperature. Because of the experimental requirement of a rather good temperature stability during the measurement ($\Delta T \leq 0.05$ K) and the relatively high reactivity of Cr, it was not possible to measure the entire temperature series within a single experimental run using the same tip and the same sample surface. Instead, each data set shown in Fig. 7 represents a new preparation, which includes the Cr sample as well as the Fe-coated tip.

Beginning with the left column [Fig. 7(a)–7(c)], the temperature of each measurement is above the spin-flip temperature $T_{SF}$. In principle, we observe the same magnetic structure in any data set (i.e., topological antiferromagnetism, which in some cases is frustrated due to the presence of screw dislocations). The magnetic contrast—in this case the
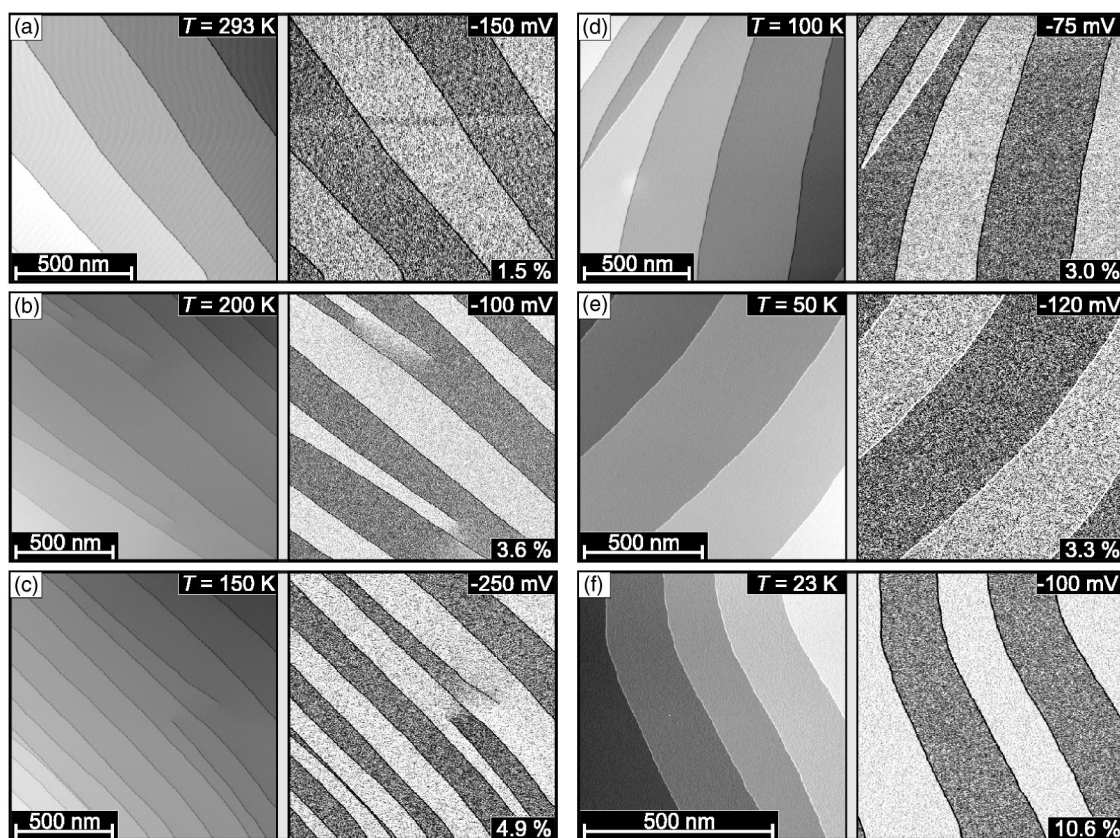
FIG. 7. Temperature-dependent SP-STM series of Cr(001) measured with an Fe-coated W tip. The topography (left) and the d$I$/d$U$ map (right) are shown for any temperature. The bias voltage $U$ and the asymmetry $P_{asym}$ are indicated in the upper- and lower-right corner of the d$I$/d$U$ map, respectively.

asymmetry of the d$I$/d$U$ signal with tip and surface spins parallel ($\sigma_{\uparrow\uparrow}$) and the signal with spins antiparallel ($\sigma_{\uparrow\downarrow}$)—is given by

$$P_{asym} = \frac{\sigma_{\uparrow\uparrow} - \sigma_{\uparrow\downarrow}}{\sigma_{\uparrow\uparrow} + \sigma_{\uparrow\downarrow}} \qquad (5)$$

and varies between 1.5% and about 5%. As already mentioned in Sec. II C, a quantitative discussion of the achieved d$I$/d$U$ contrast is difficult as the data were measured with different tips that exhibit different spin-dependent electronic properties. Therefore, the differences in the d$I$/d$U$ contrast may be the result of a nonsystematic variation of the tip's spin-polarization or of the angle $\phi$ between the tip and the sample magnetization directions rather than a systematic increase because of the reduction of the temperature. The right column [Figs. 7(d)–7(f)] shows data that were measured at temperatures below $T_{SF}$. Surprisingly, the d$I$/d$U$ map in Fig. 7(d) exhibits the same magnetic structure as the images in Figs. 7(a)–7(c). Even down to 23 K [Fig. 7(f)] there is no general change in the magnetic structure with adjacent terraces having an antiparallel magnetization. The asymmetry varies between about 3% at 100 K and 10.6% at 23 K.

Since we know from the neutron-scattering experiments that the bulk of this particular Cr crystal exhibits a spin-flip transition at the expected spin flip temperature $T_{SF}$, the SP-STM data of Fig. 7 are quite surprising. According to the simple scenarios outlined in Fig. 2 we expected that below $T_{SF}$ either the surface magnetization becomes perpendicular (out-of-plane) or that the SDW propagates within the surface plane, leading to a periodic magnetization modulation. Obviously, both proposals sketched in Figs. 2(b) and 2(c) are not in agreement with our experimental observations.

In general, the easy magnetization axis of thin film tips used in SP-STM experiments is mainly determined by the material-specific surface and interface anisotropies.[16,30] The magnetization direction of Fe-coated tips, which were used for the experiments described here, was found to be particularly reproducible perpendicular to the tip axis, i.e., within the sample's surface plane. Occasionally, however, we observed single tips with an odd magnetization direction that was not in agreement with the expected one. Furthermore, it has been demonstrated that in some cases intra-atomic non-collinear magnetism leads to a bias dependence of the tip's spin-density orientation, i.e., some tips are in-plane sensitive at one bias voltage but out-of-plane sensitive at another bias voltage.[31]

In order to exclude that the contrast observed below $T_{SF}$ in Figs. 7(d)–7(f) is caused by out-of-plane topological antiferromagnetism, we performed a comparative study on the well-studied magnetic model system of two-monolayer (ML) Fe on W(110) serving as a reference sample.[35,36] Fe grows in the step-flow mode, i.e., the W substrate's step edges are decorated with Fe nanostripes of alternating monolayer and

double-layer thickness.[37] The Fe double-layer nanostripes exhibit an out-of-plane easy axis with stripe domains running along the $1\bar{1}0$ direction.[35–37] As the up or down magnetized stripes are about 25 nm wide, the lateral magnetic periodicity along the [001] direction amounts to $\approx$50 nm. The stripe domains are separated by 180° domain walls.[36] Within the domain walls the magnetization continuously rotates thereby passing one magnetically hard in-plane orientation.[35]

In the comparative study we have coated a clean W tip with about 10 ML Fe. Upon preparation the tip was transferred into the STM. With this tip we have measured Fig. 8(a), which shows the topography of an almost perfect Fe double layer grown on a stepped W(110) substrate at about $T=450\pm50$ K. The measurement temperature during the entire cycle was 40 K. In the bottom part of Fig. 8(b) the simultaneously acquired map of the spin-resolved differential tunneling conductance $dI/dU$ at $U=-50$ mV is shown. About 7 nm wide bright and dark lines running along the $1\bar{1}0$ direction can be recognized being characteristic for domain walls as imaged with an in-plane sensitive tip.[36] Additionally, dislocation lines are also visible as dark lines along the [001] direction.

In the second step of the comparative study, we have replaced the Fe/W(110) sample by the Cr(001) sample while leaving the tip unchanged. Figure 8(c) shows the spin-resolved $dI/dU$ map of the Cr(001) surface as measured at $U=-100$ mV with the sample held at $T=40$ K. One can recognize the typical contrast between adjacent terraces as already described in Figs. 6 and 7. Since we have shown in Fig. 8(b) on Fe/W(110) that this particular Fe-coated tip is magnetically in-plane sensitive, we can now conclude that the Cr moments of the (001) surface are still in-plane although we are far below $T_{SF}$. In order to exclude that the magnetization changed between taking the data of Figs. 8(b) and 8(c) we have replaced the Cr(001) sample by the originally used Fe/W(110) sample again [Figs. 8(d) and 8(e)]. In fact, the tip still shows an in-plane sensitivity [Fig. 8(e)]. After accomplishing this experimental cycle we have provided strong evidence that the Cr(001) surface exhibits an in-plane magnetization even far below the spin-flip temperature $T_{SF}$.

## IV. DISCUSSION

In Sec. III we have shown by neutron scattering that the the particular Cr(001) crystal used in this study exhibits SDWs along the polar direction and one longitudinal direction, i.e., $L$ and $K$, respectively. Although we have not performed measurements that are sensitive to the second longitudinal direction $H$, which is equivalent to $K$, we can conclude that the bulk properties of this Cr(001) crystal are well described by a SDW state in poly-$\vec{Q}$ mode. All three propagation directions for the L-SDW as for the T-SDW along the equivalent {001} directions were observed by neutron scattering. On the Cr(001) surface, in contrast, we find a single $\vec{Q}$ state with the propagation direction perpendicular to the surface. This result is in agreement with previous x-ray and neutron-scattering studies, which observed single $\vec{Q}$
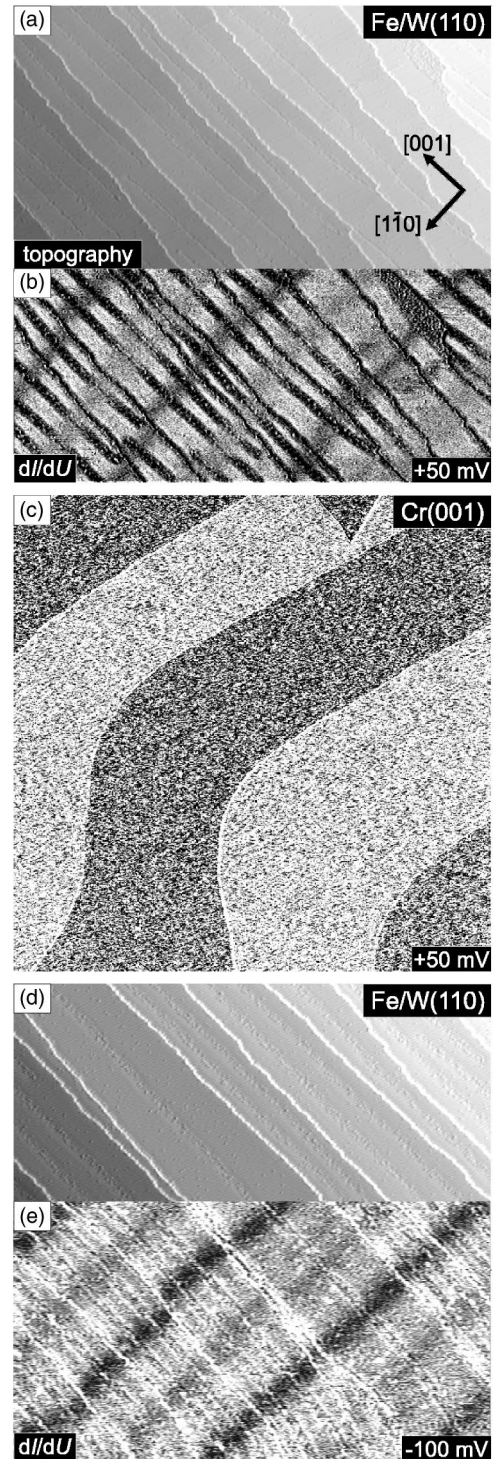


FIG. 8. Experimental cycle as described in the text to determine the orientation of the magnetization of the Cr(001) surface at 40 K. (a) and (b) show the topography and $dI/dU$ map of a two-ML Fe/W(110) test sample. (c) and (d) $dI/dU$ maps of of Cr(001). (d) and (e) again the test-sample Fe/W(110).

states on a large variety of Cr(001) surfaces and interfaces.[18–20,38] This near-surface region was determined to have an extension of $\approx1~\mu$m.

Our neutron-scattering experiments also confirm that the bulk of our Cr crystal exhibits the spin-flip reorientation. The

phase transition was found at $T_{SF}=125\pm5$ K being in good agreement with the literature value. Nevertheless, no indication of a spin-flip transition of the Cr(001) surface is observed by means of SP-STS down to $T=23$ K. Throughout the entire temperature range, both above and far below $T_{SF}$, the surface remains in-plane magnetized and no modulation of the magnetic moment is observed in the surface plane, suggesting the perpetuation of the T-SDW at the surface. Since neutron-scattering data clearly showed a L-SDW with out-of-plane magnetic moments[19] [cf. Fig. 2(b)] there seems to be an ostensible disagreement with our SP-STS results. We have to keep in mind, however, that in contrast to the neutron-scattering measurements mentioned above, which could not be performed *in situ* (i.e., at the same location where the sample preparation took place), leading to exposure to ambient conditions and oxidation, the SP-STS experiments of this study were conducted on a clean and well-defined Cr(001) surface. Probably, the oxidation of the samples used in Ref. 19 drastically changed the surface spin configuration.

Obviously, the surface magnetic structure cannot be described appropriately by a simple continuation of the bulk SDW. A possible magnetic configuration at the surface is schematically shown in Fig. 9. Here, the Cr surface layer exhibits the same magnetic structure as for $T>T_{SF}$, i.e., a T-SDW ($\vec{Q}\perp\vec{\mu}$) with $\vec{Q}$ perpendicular to the surface plane. This T-SDW with the spins in-plane forms a quasiclosure domain. A continuous connection of the surface T-SDW to the L-SDW in the near-surface region is accomplished by the formation of a 90° domain wall. The origin of the pinning of the surface magnetization within the plane may arise from a strong in-plane surface anisotropy of the Cr(001) surface. The magnetic structure of Fig. 9 is only stable if the gain of the surface anisotropy energy is higher than the energy of the 90° domain wall. In other words, the energy required for the formation of a 90° domain wall must be overcompensated by an alignment of the surface magnetization along the easy axis, which, because of surface anisotropy, is oriented parallel to the (001) plane. Based on the knowledge of the domain-wall width (cf. Fig. 6) we may speculate that the vertical extension of the 90° domain wall is on the order of a hundred to several hundreds of nanometer.

## V. SUMMARY

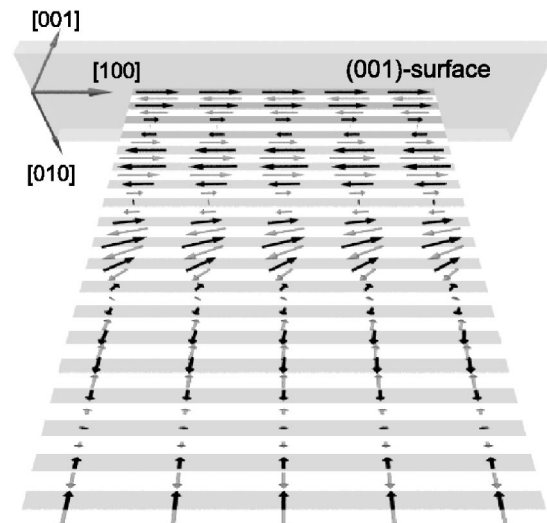In summary, we have shown by neutron scattering that the center of the Cr crystal used in the present work exhibits all



FIG. 9. Model of the low-temperature spin configuration of Cr(001). At $T<T_{SF}$ the bulk exhibits a L-SDW. A single $\vec{Q}$ state with $\vec{Q}$ perpendicular to the surface dominates in the near-surface region. The surface layer, in contrast, still exhibits a T-SDW with the magnetization lying within the surface plane. A 90° domain wall interconnects the L-SDW to the surface spins.

the known bulk characteristics. We observed a transverse incommensurate SDW above $T_{SF}$ and longitudinal incommensurate SDW below. The commensurate $AF_0$ phase was only observed at the edge of the Cr crystal. Temperature-dependent SP-STS measurements revealed that the Cr(001) surface exhibits topological antiferromagnetic order with an in-plane magnetization throughout the entire temperature range 300 K$<T\leq23$ K. No spin-flip transition is observed at the surface. This experimental result is interpreted in terms of a high surface anisotropy large enough to overcompensate the energy required for the formation of 90° domain wall that interconnects the in-plane magnetized near-surface region to the L-SDW in the bulk.

*Electronic address: mbode@physnet.uni-hamburg.de

[1] L. M. Corliss, J. M. Hastings, and R. J. Weiss, Phys. Rev. Lett. **3**, 211 (1959).

[2] P. Bödeker, A. Hucht, A. Schreyer, J. Borchers, F. Güthoff, and H. Zabel, Phys. Rev. Lett. **81**, 914 (1998).

[3] E. J. Escorcia-Aparicio, H. J. Choi, W. L. Ling, R. K. Kawakami, and Z. Q. Qiu, Phys. Rev. Lett. **81**, 2144 (1998).

[4] G. Binasch, P. Grünberg, F. Saurenbach, and W. Zinn, Phys. Rev. B **39**, 4828 (1989).

[5] M. N. Baibich, J. M. Broto, A. Fert, F. NguyenVanDau, F. Petroff, P. Eitenne, G. Creuzet, A. Friederich, and J. Chazelas, Phys. Rev. Lett. **61**, 2472 (1988).

[6] H. Zabel, J. Phys.: Condens. Matter **11**, 9303 (1999).

[7] E. Fawcett, Rev. Mod. Phys. **60**, 209 (1988).

[8] C. L. Fu and A. J. Freeman, Phys. Rev. B **33**, 1755 (1986).

[9] L. E. Klebanoff, S. W. Robey, G. Liu, and D. A. Shirley, Phys. Rev. B **30**, 1048 (1984).

[10] F. Meier, D. Pescia, and T. Schriber, Phys. Rev. Lett. **48**, 645

(1982).

[11] S. Blügel, D. Pescia, and P. H. Dederichs, Phys. Rev. B **39**, R1392 (1989).

[12] R. Wiesendanger, H. J. Güntherodt, G. Güntherodt, R. J. Gambino, and R. Ruf, Phys. Rev. Lett. **65**, 247 (1990).

[13] M. Kleiber, M. Bode, R. Ravlić, and R. Wiesendanger, Phys. Rev. Lett. **85**, 4606 (2000).

[14] M. Kleiber, M. Bode, R. Ravlić, N. Tezuka, and R. Wiesendanger, J. Magn. Magn. Mater. **240**, 64 (2002).

[15] R. Ravlić, M. Bode, A. Kubetzka, and R. Wiesendanger, Phys. Rev. B **67**, 174411 (2003).

[16] M. Bode, Rep. Prog. Phys. **66**, 523 (2003).

[17] J. Unguris, R. J. Celotta, and D. T. Pierce, Phys. Rev. Lett. **69**, 1125 (1992).

[18] J. P. Hill, G. Helgesen, and D. Gibbs, Phys. Rev. B **51**, 10 336 (1995).

[19] P. Sonntag, P. Bödeker, A. Schreyer, H. Zabel, K. Hamacher, and H. Kaiser, J. Magn. Magn. Mater. **183**, 5 (1998).

[20] P. Bödeker, A. Schreyer, and H. Zabel, Phys. Rev. B **59**, 9408 (1999).

[21] J. Meersschaut, J. Dekoster, R. Schad, P. Beliën, and M. Rots, Phys. Rev. Lett. **75**, 1638 (1995).

[22] Note, that the investigated Cr(001) surfaces were not prepared in situ but have been exposed to ambient conditions between preparation and analysis. Therefore, the surfaces are certainly oxidized and contaminated.

[23] K.-F. Braun, S. Fölsch, G. Meyer, and K.-H. Rieder, Phys. Rev. Lett. **85**, 3500 (2000).

[24] X. W. Jiang and R. S. Fishman, J. Phys.: Condens. Matter **9**, 3417 (1997).

[25] J. A. Stroscio, D. T. Pierce, A. Davies, R. J. Celotta, and M. Weinert, Phys. Rev. Lett. **75**, 2960 (1995).

[26] J. Schäfer, E. Rotenberg, G. Meigs, S. D. Kevan, P. Blaha, and S. Hüfner, Phys. Rev. Lett. **83**, 2069 (1999).

[27] A. Arrott, in *Magnetism*, edited by G. Rado and H. Suhl (Academic, New York, 1966), Vol. IIB, p. 295.

[28] S. W. Lovesey, *Theory of Neutron Scattering from Condesed Matter* (Clarendon, Oxford, 1984), Vol. 2.

[29] J. Wiebe, A. Wachowiak, F. Meier, D. Haude, T. Foster, M. Morgenstern, and R. Wiesendanger, Rev. Sci. Instrum. **75**, 4871 (2004).

[30] M. Bode, O. Pietzsch, A. Kubetzka, and R. Wiesendanger, J. Electron Spectrosc. Relat. Phenom. **114–116**, 1055 (2001).

[31] M. Bode, O. Pietzsch, A. Kubetzka, S. Heinze, and R. Wiesendanger, Phys. Rev. Lett. **86**, 2142 (2001).

[32] J. C. Slonczewski, Phys. Rev. B **39**, 6995 (1989).

[33] S. A. Werner, A. Arrott, and H. Kendrick, Phys. Rev. **155**, 528 (1967).

[34] A. Hubert and R. Schäfer, *Magnetic Domains* (Springer, New York, 1998).

[35] M. Bode, S. Heinze, A. Kubetzka, O. Pietzsch, X. Nie, G. Bihlmayer, S. Blügel, and R. Wiesendanger, Phys. Rev. Lett. **89**, 237205 (2002).

[36] A. Kubetzka, O. Pietzsch, M. Bode, and R. Wiesendanger, Phys. Rev. B **67**, 020401(R) (2003).

[37] H. J. Elmers, J. Hauschild, and U. Gradmann, Phys. Rev. B **59**, 3688 (1999).

[38] P. Sonntag, P. Bödeker, T. Thurston, and H. Zabel, Phys. Rev. B **52**, 7363 (1995).